Sensors and Materials, Vol. 36, No. 6 (2024) 2209–2224
MYU Tokyo

S & M 3663

Strain Sensorization of a Bladder of Expanding Pouch Actuator Using Liquid Metal

Seiichi Yamamoto,[1] Hiroki Ishizuka,[1*] Takefumi Hiraki,[2]
Sei Ikeda,[1] and Osamu Oshiro[1]

[1]Graduate School of Engineering Science, Osaka University,
1-3 Machikaneyama, Toyonaka, Osaka 560-8531, Japan
[2]Metaverse Lab, Cluster, Inc., 8-9-5 Nishigotanda, Shinagawa-ku, Tokyo 141-0031, Japan

(Received January 31, 2024; accepted April 19, 2024)

Keywords: soft robot, soft sensor, strain sensor, liquid metal, pouch actuator

Soft pneumatic pouch actuators with simple structures and fabrication processes are being studied for application in soft robots. In addition, some research groups have tried to add sensors to the pouch actuators to estimate their states. In this study, we propose to embed a soft strain sensor made of liquid metal in the bladder of a pouch actuator made of stretchable styrene–ethylene–butadiene–styrene (SEBS) film, which can expand to a large extent under pressure to enable shape estimation. A method of processing the bladder of the pouch actuator to convert it into a sensor has yet to be proposed. We developed a fabrication process to form the small strain sensor in the SEBS film and evaluated the strain sensor's stretch characteristics. Finally, we confirmed that the deformation of a bending pouch actuator caused by pneumatic pressure is expressed in the electrical resistance of the embedded strain sensor.

1. Introduction

Soft robots have been actively developed for applications in extreme environments and cooperative work.[1,2] To accomplish these tasks, it is necessary for soft robots to perceive and understand the external environment as well as their state. For this purpose, soft actuators are needed to perform the desired motions and soft sensors to measure their states are necessary. The principles of soft actuators include pneumatic pressure,[3] hydraulic pressure,[4] shape memory alloys,[5] and liquid crystal elastomers.[6] Soft pneumatic actuators, which convert the energy of compressed air into various types of motion such as extension,[7] bending,[8] and torsion,[9] are widely used for soft robots because of their light weight and high power-to-weight ratio.[10] A specific type of thin and planar pneumatic actuator is called the pouch actuator, which has attracted attention owing to its cost-effectiveness and ease of fabrication.[11–14] The pouch actuator consists of non-stretchable thermoplastic films, such as nylon or polyethylene, and is fabricated by thermally bonding the plastic films together to form a bladder. Typically, the thermoplastic films allow for limited elongation compared with the silicone rubber used to

*Corresponding author: e-mail: Ishizuka@bpe.es.osaka-u.ac.jp
https://doi.org/10.18494/SAM5009

ISSN 0914-4935
https://myukk.org/

fabricate soft pneumatic actuators. When using the pouch actuator, its motion design primarily relies on its contraction behavior induced by its structure. The achievement of various motions using external attachments[15,16] and an origami structure[17,18] have been explored. Arfaee *et al.* recently applied a styrene–ethylene–butylene–styrene (SEBS) block copolymer film with high stretchability and thermoplasticity[19] to the pouch actuator. SEBS films, which have approximately ten times the stretchability of the previously used plastic films, allow the pouch actuator to stretch and expand under applied pneumatic pressure, similar to silicone rubber actuators. By using SEBS films in the pouch actuator, it is possible to explore and design motion based on stretch, making expansion possible.

In particular, when expanding pouch actuators made of SEBS film undergo significant deformation resulting in stretching, there is a need for a method to measure the shape changes caused by it. Previously, pouch actuators were primarily composed of non-stretchable materials, leading to considerations mainly focused on pressure measurement and contact detection using sensors.[20–22] Combining sensors to measure the deformation of pouch actuators is conceivable as a method to measure stretching. Kim *et al.* proposed a method using conductive fabrics and capacitance measurement to measure the contraction of pouch actuators.[23] However, existing products such as Soft Flex and Kim's method utilize sensors made of non-stretchable materials, making it difficult to measure the stretching of actuators like expanding pouch actuators. Additionally, there is a problem of compromising their flexibility or constraining deformation. Therefore, it is desirable to place flexible and stretchable sensors in pouch actuators similar to conventional soft actuators.[24] Numerous studies have been conducted to fabricate flexible and stretchable sensors by embedding conductive materials into flexible materials such as silicone rubber.[25,26] When these sensors are attached to pouch actuators, deformation may be constrained or these sensors are detached owing to the difference in Young's modulus between materials.[27]

On the basis of the current situation outlined above, this study proposes a method to sensorize the flexible and stretchable SEBS bladder itself, which forms the expanding pouch actuator, to measure its stretching (Fig. 1). Research on functionalizing the bladder itself for sensing purposes has not been conducted yet. The proposed method is inspired by existing studies on soft sensors using liquid metals.[28,29] It involves forming small channels inside the SEBS film and filling them with liquid metal to form strain sensors, thereby sensorizing the bladder. When the film deforms, the channels deform as well, resulting in changes in the shape of the liquid metal strain sensor. By measuring the resistance change of the strain sensor, deformation can be estimated. This method functionalizes the bladder without needing expensive equipment such as a photolithography system, using wire-based molding techniques.[30–32] This process can be integrated into the process of fabricating pouch actuators. The cost of the sensor is approximately 10 cents, much cheaper than using off-the-shelf sensors.[33] Moreover, since different materials are not used for the sensor substrate, there is no issue of sensor detachment from the actuator. The contributions of this study are as follows:

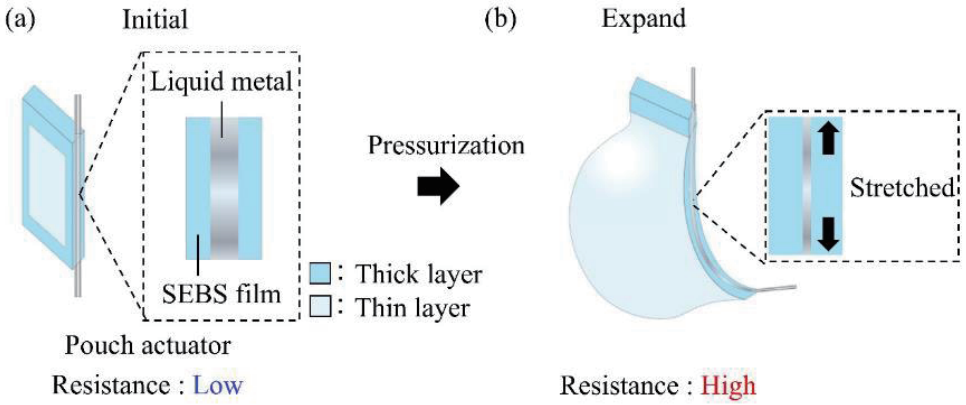

Fig. 1. (Color online) Application of the proposed strain sensor embedded in a SEBS film. The strain sensor is used to estimate the deformation of a bending pouch. (a) Configuration of the strain sensor embedded in the bending pouch actuator. (b) The shape and electrical resistance of the strain sensor change with deformation due to applied pneumatic pressure.

- We propose a method to sensorize the bladder of the expanding pouch actuator by forming a strain sensor within the stretchable film to measure deformation.
- We fabricated a strain sensor within the SEBS film and confirmed the relationship between the applied strain and the resistance change.
- We fabricated a bending expanding pouch actuator embedded with a strain sensor to explore the design space and confirmed the relationship between the bending angle and the resistance change.

2. Theory and Fabrication

In this section, we describe the design of a strain sensor embedded in a bladder. First, we describe the structure and principle of the strain sensor and give its dimensions. Then, we show the fabrication process used.

2.1 Principle and theory

As shown in Fig. 2, the liquid-metal-based strain sensor formed within the SEBS film undergoes shape changes due to the stretching of the film. A microchannel within the SEBS film is filled with 0.21-mm-diameter liquid metal, forming the strain sensor [Fig. 2(a)]. The cross-sectional area of the liquid metal channel is 0.35 mm^2 and its length is 34 mm. The ends of the strain sensor are connected to metal wires, and the electrical resistance is measured through these wires. The initial electrical resistance of the liquid metal strain sensor can be expressed as

$$R_0 = \rho \frac{L_0}{S_0}, \tag{1}$$

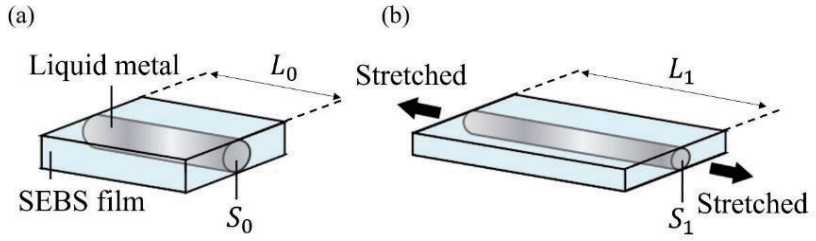

Fig. 2. (Color online) Principle of strain sensor. (a) The strain sensor is formed in a stretchable SEBS film using an embedded channel filled with liquid metal. (b) When the SEBS film is stretched, the shape of the strain sensor within the film changes, resulting in a change in electrical resistance. The change in electrical resistance can be used to estimate the amount of film stretching.

where R_0, ρ, S_0, and L_0 represent the initial electrical resistance, the electrical resistivity of the liquid metal, the initial cross-sectional area, and the initial length, respectively. The resistivity of the liquid metal is 29.4 × 10^{-8} Ω·m.[34] As the film is stretched, the shape of the microchannel changes, causing a corresponding change in the shape of the liquid metal filling the inside [Fig. 2(b)]. The liquid metal is incompressible, so even when subjected to external force and deformation, the volume of the liquid metal remains constant. Therefore, the total length increases while the cross-sectional area decreases. Given that the volume of the liquid metal is invariant, the electrical resistance of the liquid metal when an external force is applied can be expressed as

$$R_1 = \rho \frac{L_1}{S_1} = \rho \frac{{L_1}^2}{L_0 S_0}, \tag{2}$$

where R_1, S_1, and L_1 represent the electrical resistance, cross-sectional area, and length after the film is stretched. By defining the strain of the sensor $\left(\frac{L_1 - L_0}{L_0}\right)$ as ε, the change in electrical resistance, ΔR, can be expressed as

$$\begin{aligned} \Delta R = R_1 - R_0 &= \rho \frac{{L_1}^2 - {L_0}^2}{L_0 S_0} = \rho \frac{L_0}{S_0} \frac{L_1 - L_0}{L_0} \left(\frac{L_1}{L_0} + 1 \right) \\ &= \rho \frac{L_0}{S_0} \frac{L_1 - L_0}{L_0} \left(\frac{L_1 - L_0}{L_0} + 2 \right) = \rho \frac{L_0}{S_0} \varepsilon (\varepsilon + 2). \end{aligned} \tag{3}$$

Using this equation, it is possible to derive a theoretical value of the change in electrical resistance due to stretching.

2.2 Fabrication process

Figures 3(a)–3(d) illustrate the process of fabricating a strain sensor embedded in a SEBS film. This fabrication process mainly requires only thermal bonding, which makes it simple and inexpensive. Two 0.2-mm-thick SEBS films (SEBS film, Vreeberg Elastic Materials) were sandwiched together with a 0.21-mm-diameter metal wire (tin-plated annealed copper wire, RS Components) as a mold. They were then thermally bonded [Fig. 3(a)]. Subsequently, the metal wire was removed to form a hollow channel [Fig. 3(b)]. The melted film had a thickness of about 0.4 mm. The channel formed by the metal wire was filled with the liquid metal EGaIn [75% Ga and 25% In by weight)][35] using a syringe [Fig. 3(c)]. Finally, metal wires were inserted [Fig. 3(d)]. The actual sensor and its size are shown in Fig. 3(e).

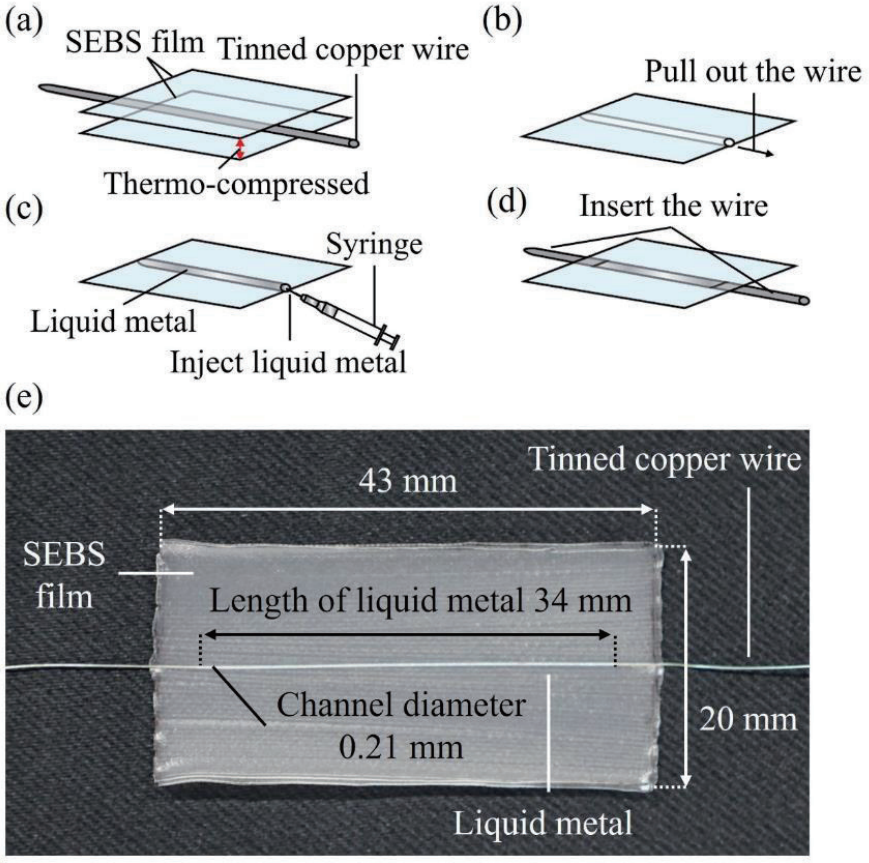

Fig. 3. (Color online) Process of fabricating the strain sensor. (a) Thermal bonding of SEBS film. (b) Formation of a hollow channel by wire drawing. (c) Formation of a strain sensor by injecting liquid metal into the channel. (d) Insertion of wires for measurement. (e) Photograph of the fabricated sensor and its size.

3. Experimental Procedure

Here, we describe the experimental method used to characterize a strain sensor and its implementation in a bending pouch actuator.

3.1 Characterization

The response of the strain sensor to strain was evaluated. The experimental setup used for the response evaluation is shown in Fig. 4(a). The experimental setup consisted of a linear actuator (CBX1605-200A, Rattmmotor), a linear encoder (DS-025, Mutoh Industries), an LCR meter (IM3533, Hioki), two microcontrollers (Arduino Mega R3 2560, Arduino LLC), and two laptop computers. The linear actuator was controlled to move in a straight line in accordance with the signals sent from the laptop computer (Yoga 6 13ALC7, Lenovo) via the microcontroller. The linear encoder measured the position of the actuator and sent it to the other computer (Surface laptop 4, Microsoft) via another microcontroller. The electric resistance of the strain sensor was transmitted from the LCR meter to the laptop computer via serial communication.

First, the relationship between strain and the change in electrical resistance was investigated. The electrical resistance was recorded when the film and strain sensors were stretched at a strain of 0 (0 mm), 5 (1.7 mm), 10 (3.4 mm), 15 (5.1 mm), 20 (6.8 mm), 25 (8.5 mm), 30 (10.2 mm), or

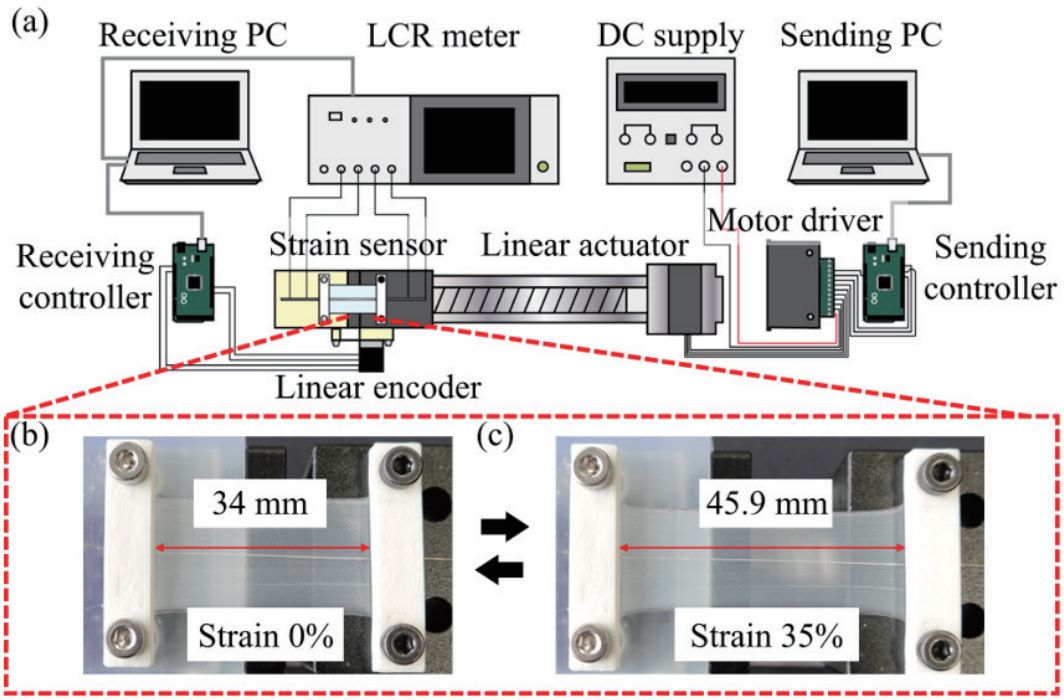

Fig. 4. (Color online) Experimental setup. (a) The sensor was stretched using a linear actuator, and the displacement and resistance were measured using a linear encoder and an LCR meter. (b) Initial state of the strain sensor. (c) State of the strain sensor stretched at strain of 35%.

35% (11.9 mm) and a speed of 0.95 mm/s. Measurements were performed five times for each strain condition. Next, the dynamic characteristics of the sensor were investigated, focusing on hysteresis and the effect of strain rate. The film and strain sensor were stretched at a strain of 35% [Figs. 4(b) and 4(c)] and then returned to the initial state to obtain the hysteresis loop. The strain rate was 0.95 mm/s. In addition, we evaluated the effect of speed on the change in electrical resistance. The electrical resistance was recorded when the strain was 35%. The actuator speed was 0.95, 1.9, or 3.6 mm/s. Finally, the film and strain sensor were subjected to repeated strain cycles of 35% at a speed of 0.95 mm/s for 100 iterations, and the electrical resistance was recorded during this process. We calculated the change in electrical resistance from the initial value.

3.2 Application

To verify the proposed method and explore the design space of the expanding pouch actuator, we fabricated a bending pouch actuator with a strain sensor. Subsequently, we evaluated the relationship between the bending angle and the sensor output. The principle of the bending pouch actuator is the same as shown in Fig. 1. In the study by Arfaee *et al*.,[19] only a simple-shaped pouch actuator using a SEBS film was fabricated. However, by designing the stretchiness of the material, it is possible to fabricate an expanding pouch actuator capable of various deformations. The bending pouch actuator in this study consists of thin and thick surfaces with a strain sensor embedded in the side [Fig. 1(a)]. Designing a structure within the bending pouch actuator with stretch-resistant and stretchable surfaces makes it capable of bending actuation. When pneumatic pressure is applied to the bending pouch actuator, the thin surface is stretched more than the thick surface [Fig. 1(b)]. This difference in deformation causes the pouch actuator to bend. The embedded strain sensor is stretched by the deformation and the change in shape causes the change in electrical resistance.

Figure 5 shows the fabrication process used. Two SEBS films 0.2 mm thick were thermally bonded to form a thicker SEBS film [Fig. 5(a)]. The thicker SEBS film and a SEBS film were then thermally bonded with a 0.21-mm-diameter metal wire in between [Fig. 5(b)]. The edges of the thicker SEBS film and a SEBS film were thermally bonded together, sandwiching a sheet of paper as an air inlet [Fig. 5(c)]. The paper and metal wire were then removed [Fig. 5(d)]. The channel formed by the metal wire was filled with liquid metal using a syringe to form the strain sensor [Fig. 5(e)]. Two metal wires were inserted at both ends of the strain sensor [Fig. 5(f)]. A silicone tube was inserted to provide pneumatic pressure [Fig. 5(g)]. The gap between the silicone tube and the SEBS film was filled with adhesive to prevent air leakage. An actual photograph of the bendable pouch actuator is shown in Fig. 5(h). The fabricated pouch actuator had dimensions of approximately $20 \times 43 \times 0.8$ mm^3, with a width of approximately 4.5 mm for the heat-sealed ends. The inserted tube had an outer diameter of 4 mm and an inner diameter of 2 mm.

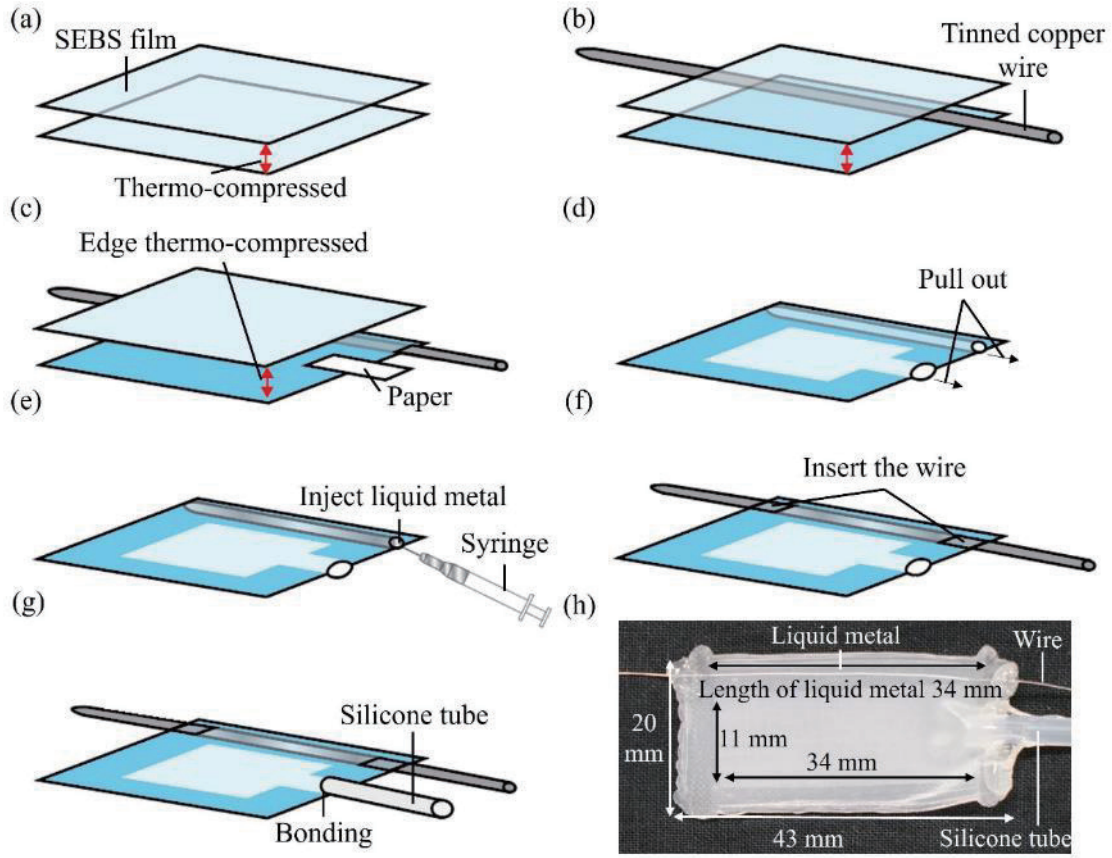

Fig. 5. (Color online) Process of fabricating bending pouch actuator. (a) Thermal bonding of SEBS film. (b) Thermal bonding of SEBS film sandwiching a metal wire. (c) Thermal bonding of SEBS film to form the bending actuator. (d) Formation of a hollow channel and air inlet by wire and paper insertion. (e) Formation of a strain sensor by injecting liquid metal into the channel. (f) Insertion of wires for measurement. (g) Insertion of a silicone tube to apply pneumatic pressure. (h) Photograph of the finished bending pouch actuator.

We evaluated the relationship between bending angle and sensor output to assess its performance. Figure 6 illustrates the experimental setup used to evaluate the relationship between angle and output. In the experiment, we connected the strain sensor to an LCR meter (IM3533, Hioki) with metal wires. Pneumatic pressure was applied to the bending pouch actuator with a syringe (60 mL disposable syringe, Narika), and the pouch actuator's bending angle was measured using a video camera (FDR-AX700, SONY). The recorded video was divided into frames, and the bending angle was derived from the images. The resistance displayed on the LCR meter in each frame was also recorded. After the measurement, we calculated the change in electrical resistance from the initial value.

Then, the repeatability was evaluated. Figure 7 illustrates the experimental setup for repeatability. The experimental setup consisted of an air compressor (SR-102, Fujiwara Sangyo), an electro-pneumatic regulator (EVD-1100-008AN, CKD), a microcontroller (Arduino Mega R3 2560, Arduino LLC), and a solenoid valve (VQ110U-6L0, SMC), all connected to a power supply

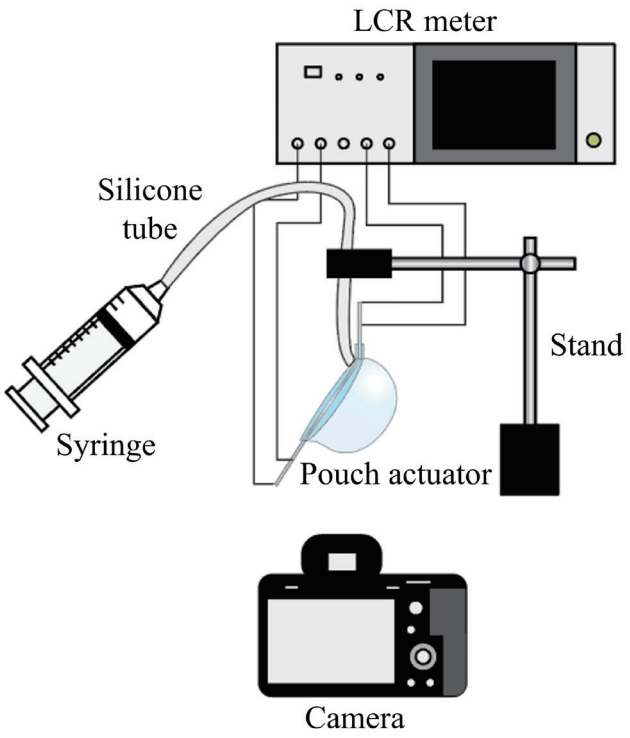

Fig. 6. (Color online) Experimental setup of the bending pouch actuator. The pouch actuator was bent by applying pneumatic pressure through a syringe. The deformation of the pouch actuator and the electrical resistance of the strain sensor were observed using a camera and an LCR meter.

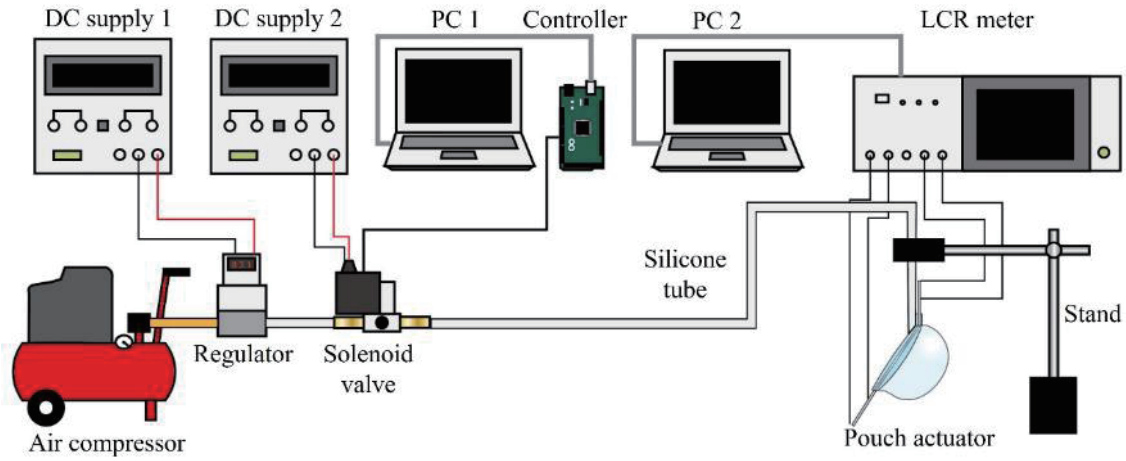

Fig. 7. (Color online) Experimental setup for repeatability. The setup involves regulating the compressed air generated by an air compressor using an electronic pressure regulator. By opening and closing a solenoid valve, pressure is repeatedly applied and released to the pouch actuator. The resistance change of the pouch actuator during this process is measured using an LCR meter.

(IPS303DD, ISOTECH). The strain sensor was connected to the LCR meter. Initially, compressed air of 21 kPa was generated using the air compressor. The solenoid valve was opened and closed to fill and release compressed air to the pouch actuator. The state of the solenoid valve was controlled using the microcontroller. The valve was set to open for 3 s and close for 10 s, and the resistance of the sensor was measured using the LCR meter during the repeated opening and closing cycles. Each cycle was repeated ten times. After the measurements, the changes in resistance were derived.

4. Results and Discussion

4.1 Characterization

The resistance changes in each strain state were measured five times and the standard deviation was derived from these results. This was plotted on the graph as error bars [Fig. 8(a)]. The standard deviation is very small, indicating that the error bars overlap with the points on the graph. The average maximum resistance change of the sensor is consistent with the theoretical value calculated by Eq. (3), demonstrating an approximately linear relationship between the changes in electrical resistance and the strain induced by stretching [Fig. 8(a)]. This indicates that the electrical resistance changed in accordance with the theoretical model, and the strain of the film can be estimated from the changes in electrical resistance. The electrical resistance was confirmed to increase linearly under the experimental condition by linear approximation. However, it should be noted that the relationship between the change in electrical resistance and strain is nonlinear, as shown in Eq. (3), and a linear approximation becomes difficult, especially when the sensor is significantly stretched.

A small hysteresis loop was observed in the relationship between changes in electrical resistance and strain [Fig. 8(b)]. The hysteresis was about 0.16% and was attributed to the excellent hysteresis characteristics of SEBS under small strain conditions.[36] Figure 8(c) shows that the strain rate of the film and strain sensor does not significantly affect the change in electrical resistance. Within the range of speeds tested, the film and liquid metal were able to deform and follow the strain induced by the stretch. This observation is consistent with those in previous studies on silicone rubber materials and liquid metal sensors where the stretching speed did not affect the resistance changes.[37] When the film was repeatedly stretched to induce strain, the change in electrical resistance due to strain was always about 0.25 Ω [Fig. 8(d)]. This indicates that the strain sensor embedded in the proposed SEBS film has high strain repeatability, which can be attributed to the flexibility of the materials of the strain sensor. In this study, the experiments were conducted within the elastic deformation range of the film. However, if the applied strain exceeds the elastic limit and causes plastic deformation, it is expected that the shape of the strain sensor will also change. In such cases, the observed repeatability may not be maintained. The SEBS film used in this study has an elongation at a break of 690%. Therefore, it is assumed that the bladder with the strain sensor can withstand elongation up to this level. However, in our preliminary experiments, we observed the plastic deformation of the strain sensor when the strain exceeds 35%. It is desirable to use the sensor at strain levels below this threshold to prevent plastic deformation.

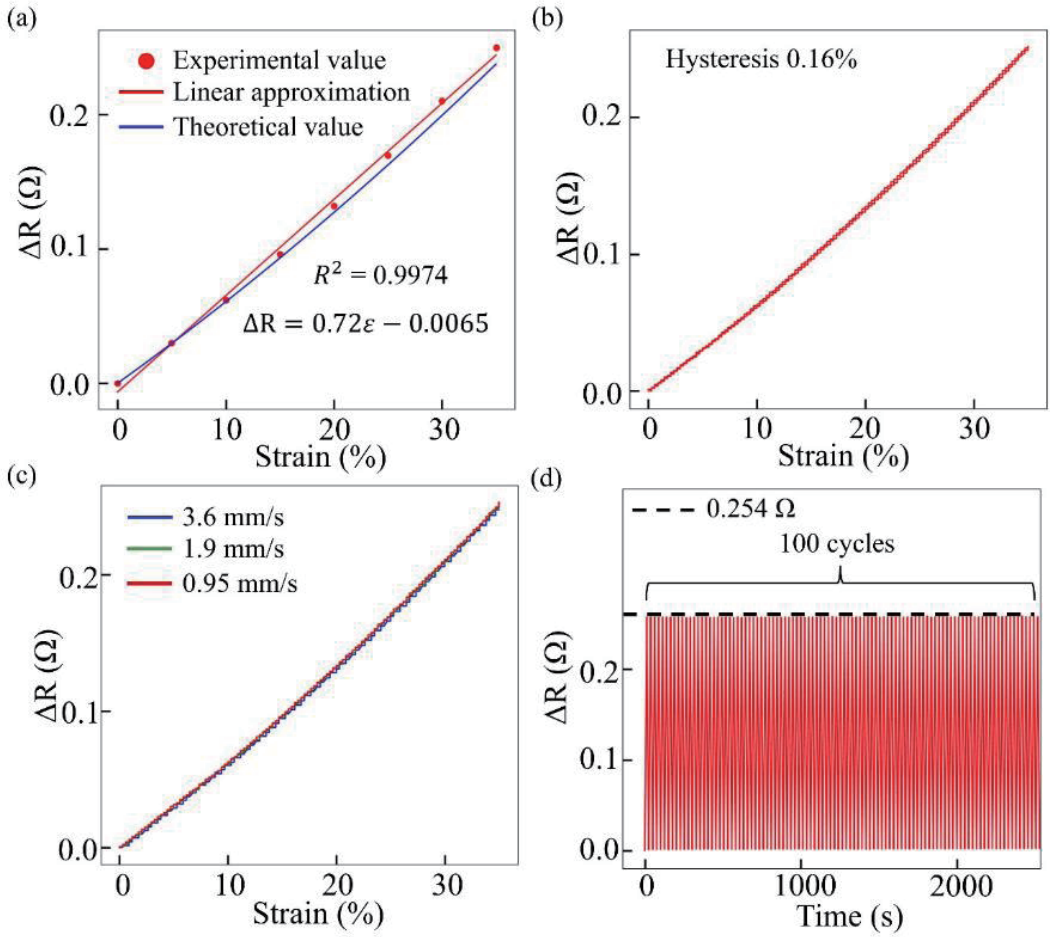

Fig. 8. (Color online) Characterization results. (a) The observed result is in agreement with the theoretical result, confirming that the strain sensor has the expected deformation. The high coefficient of determination indicates linearity in the relationship between strain and the change in electrical resistance. (b) The proposed sensor showed a small hysteresis loop. We believe that the small hysteresis was a result of the flexibility of the materials. (c) The stretching speed did not affect the resistance change of the strain sensor. (d) Even when the film was stretched 100 times at an elongation of 35%, the response of the sensor remained unchanged.

The proposed fabrication process has been confirmed to enable the fabrication of a strain sensor within a stretchable film, which allows the measurement of film strain as a change in electrical resistance, from the experimental results. It is possible to fabricate strain sensors of different sizes by varying the size of the metal wire used as the mold. For example, reducing the diameter of the strain sensor by using a metal wire with a smaller diameter could increase the resistance and improve the sensitivity. Even if strain sensors of different dimensions are fabricated, it should be possible to theoretically calculate them using Eq. (3).

4.2 Application

From Fig. 9, we confirmed that the deformation of the bending pouch actuator induced by pneumatic pressure changed the electrical resistance of the strain sensor. In contrast to conventional studies,[38] in which bending pouch actuators with complex designs were proposed, in this study, we successfully developed a bending pouch actuator with a simple structure facilitated by the stretchability of the bladder. The consideration of stretchability in the design and fabrication of the pouch actuator allowed us to achieve the desired actuation. While this study focused on stretching actuation, it is anticipated that considering stretchability can also realize various other actuations.

The bending angle of the bending pouch actuator is defined as shown on the right side of Fig. 9. The decrease in electrical resistance at a bending angle of 0 degrees was attributed to the initial inflow of air, causing the bending pouch actuator to expand in the thickness direction and compress on the sides. This phenomenon was observed in studies involving soft actuators embedded with other soft sensors.[39] Subsequently, as the internal pressure increased, the bending pouch actuator expanded in all directions. As a result, the resistance increased. Owing

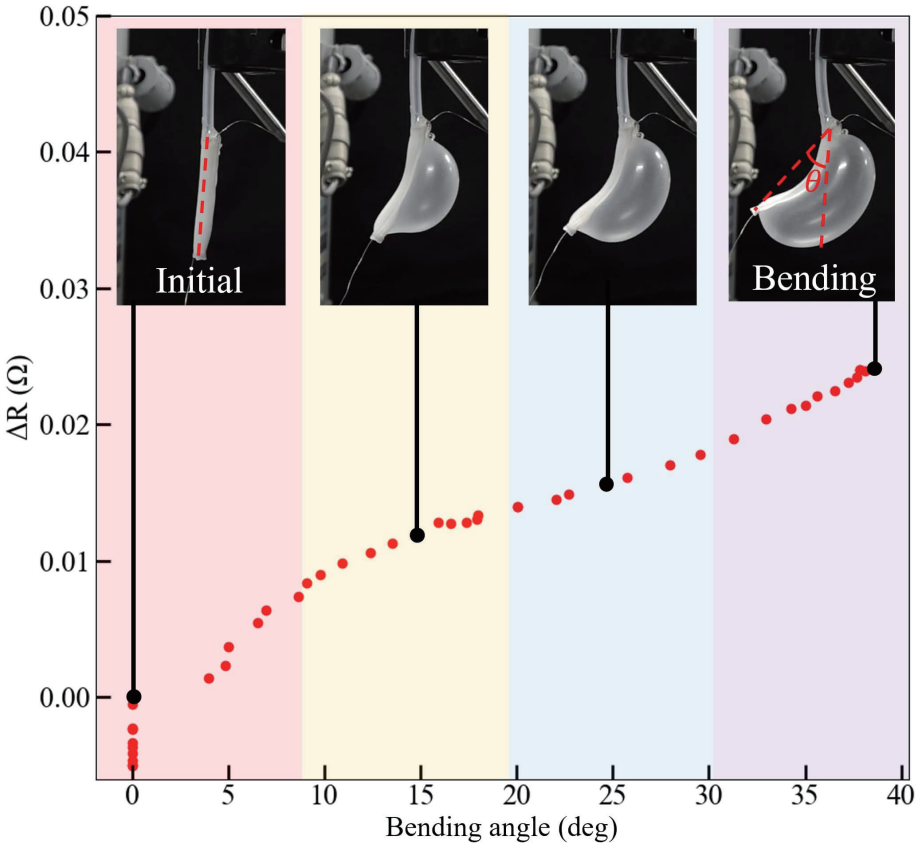

Fig. 9. (Color online) Relationship between bending angle and resistance change of the bending pouch actuator. At a bending angle of 0 degrees, the resistance change was negative. Subsequently, as the actuator began to bend under pressure, the resistance increased.

to the difference in the amount of film stretching, the bending pouch actuator started to bend at this stage. Eventually, the bending pouch actuator reached a maximum bending angle of approximately 40 degrees. The resistance increased with the bending angle, indicating that deformation can be estimated from the resistance change. With further advancements in pouch actuator research and sufficient modeling, it may be possible to derive the relationship between resistance and deformation beforehand. Additionally, Fig. 10 shows the change in electrical resistance when the bending pouch actuator is bent repeatedly ten times. Measurements were initiated after pressurizing and depressurizing once to maintain the internal pressure of the actuator. The results demonstrate high repeatability in measuring the bending pouch actuator's bending actuation. Additionally, we investigated the effect of forming the strain sensor on the actuation of the bending pouch actuator under the same pressure, and the results are shown in Fig. 11. From these results, it can be observed that forming the strain sensor resulted in approximately a 15° difference in bending angle. This difference is believed to be caused by the wires connecting the LCR meter to the strain sensor. This effect can be reduced by designing the pouch actuator so that the metal wires do not constrain the deformation.

Although this study focused on bending pouch actuators using SEBS films, the proposed method can be widely applied to pouch actuators made of stretchable thermoplastic films, opening up new possibilities in the field. In the future, when materials with superior performance are developed or when fabricating pouch actuators with more complex shapes, the proposed method can be utilized to form sensors within the pouch actuator. When actually using pouch actuators, the pouch actuators may deform and the resistance may change owing to contact with external objects. This problem of distinguishing between contact and posture states of soft actuators has been reported even when incorporating other strain sensors.[40] To address this issue, Sun *et al.* successfully incorporated sensors to detect contact in addition to strain sensors

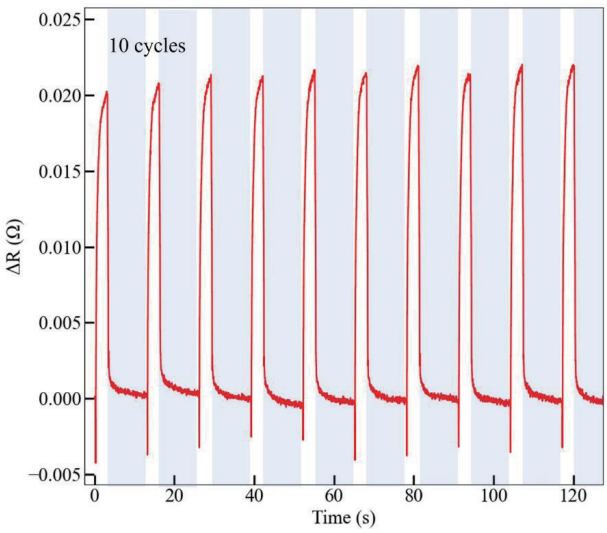

Fig. 10. (Color online) Relationship between resistance change and time when the bending pouch actuator was bent repeatedly for ten cycles. The bending pouch actuator fabricated in this study demonstrated repeatability under the experimental conditions.

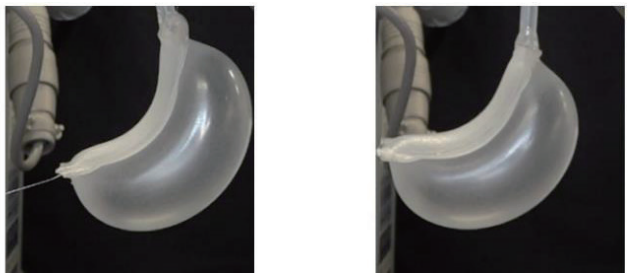

(a) (b)

Fig. 11. (Color online) Effect of forming the strain sensor in the bladder on the actuation of the pouch actuator. The results revealed an approximately 15° difference in bending angle between the pouch actuators (a) with and (b) without the strain sensor.

and achieved the separation of bending and contact detection using machine learning.[41] By incorporating this approach into the present actuator, there may be potential to separate and identify bending and contact in the future, a promising development that could revolutionize the field of soft robotics. This would require the incorporation of multiple sensors, and in cases where numerous sensors are required, a method such as screen printing may be necessary to produce multiple sensors simultaneously.[42]

5. Conclusions

In this study, we developed the method of sensorizing a stretchable and flexible thermoplastic bladder by forming liquid metal-based strain sensors. The proposed fabrication process was successfully demonstrated. Through characterization experiments, it was confirmed that the relationship between the applied strain and the resistance change of the strain sensor is close to the theoretical one and that a linear approximation is valid for strain levels up to 35%. In addition, the sensor was found to have low hysteresis (0.16%) and good repeatability of cyclic strain. Finally, we fabricated a bending pouch actuator with a strain sensor by thermally bonding the bladder, considering its spatial low stretchability. The results show the potential of the proposed strain sensor to monitor the deformation of a pouch actuator using a stretchable material. Additionally, the design of the pouch actuator, considering the spatial low stretchability of the bladder, suggested that the desired deformation of the pouch actuator could be achieved.

Acknowledgments

This work was supported in part by JSPS KAKENHI Grant Numbers JP20H02121, JP22H01447, and JP23H01379, and JST PRESTO Grant Number JPMJPR22S2, Japan.

References

1 W. Liu, Y. Duo, J. Liu, F. Yuan, L. Li, L. Li, G. Wang, B. Chen, S. Wang, H. Yang, Y. Liu, Y. Mo, Y. Wang, B. Fang, F. Sun, X. Ding, C. Zhang, and L. Wen: Nat. Commun. **13** (2022) 5030. https://doi.org/10.1038/s41467-022-32702-5

2 M. M. Coad, L. H. Blumenschein, S. Cutler, J. A. Reyna Zepeda, N. D. Naclerio, H. El-Hussieny, U. Mehmood, J. H. Ryu, E. W. Hawkes, and A. M. Okamura: IEEE Robot. Autom. Mag. **27** (2020) 120. https://doi.org/10.1109/MRA.2019.2947538
3 D. Ellis, M. Venter, and G. Venter: Soft Robot. **8** (2021) 478. https://doi.org/10.1089/soro.2020.0017
4 K. Suzumori, S. Iikura, and H. Tanaka: Proc. IEEE Int. Conf. Robot. Autom. **2** (1991) 1622. https://doi.org/10.1109/ROBOT.1991.131850
5 X. Huang, K. Kumar, M. K. Jawed, A. Mohammadi Nasab, Z. Ye, W. Shan, and C. Majidi: Adv. Mater. Technol. **4** (2019) 1800540. https://doi.org/10.1002/admt.201800540
6 J. M. Boothby, J. C. Gagnon, E. McDowell, T. Van Volkenburg, L. Currano, and Z. Xia: Soft Robot. **9** (2022) 154. https://doi.org/10.1089/soro.2020.0135
7 F. Connolly, P. Polygerinos, C. J. Walsh, and K. Bertoldi: Soft Robot. **2** (2015) 26. https://doi.org/10.1089/soro.2015.0001
8 J. Shintake, H. Sonar, E. Piskarev, J. Paik, and D. Floreano: Proc. IEEE/RSJ Int. Conf. Intell. Robots Syst. (2017) 6221. https://doi.org/10.1109/IROS.2017.8206525
9 S. H. Yoo, M. Kim, H. J. Park, G. I. Lee, S. H. Lee, and M. K. Kwak: Sci. Technol. Adv. Mater. **24** (2023) 2274818. https://ssrn.com/abstract=4415991
10 M. S. Xavier, C. D. Tawk, A. Zolfagharian, J. Pinskier, D. Howard, T. Young, J. Lai, S. M. Harrison, Y. K. Yong, M. Bodaghi, and A. J. Fleming: IEEE Access **10** (2022) 59442. https://doi.org/10.1109/ACCESS.2022.3179589
11 R. Niiyama, D. Rus, and S. Kim: Proc. IEEE Int. Conf. Robot. Autom. (2014) 6332. https://doi.org/10.1109/ICRA.2014.6907793
12 R. Niiyama, X. Sun, C. Sung, B. An, D. Rus, and S. Kim: Soft Robot. **2** (2015) 59. https://doi.org/10.1089/soro.2014.0023
13 Y. Nishioka, M. Uesu, H. Tsuboi, and S. Kawamura: Proc. Int. Conf. Mechatron. Mach. Vision Pract. (2012) 474.
14 Y. Akachi and J. Yamaoka: Proc. SIGGRAPH Asia 2023 Emerging Technologies, (2023) 1. https://doi.org/10.1145/3610541.3614571
15 X. Sun, S. M. Felton, R. Niiyama, R. J. Wood, and S. Kim: Proc. IEEE Int. Conf. Robot. Autom. (2015) 3160. https://doi.org/10.1109/ICRA.2015.7139634
16 C. Liu, S. M. Felton: Proc. IEEE/RSJ Int. Conf. Intell. Robots Syst. (2017) 1979. https://doi.org/10.1109/IROS.2017.8206017
17 S. Li, J. Lin, H. Kang, Y. Cheng, and Y. Chen: Robot. Auton. Syst. **149** (2022) 103983. https://doi.org/10.1016/j.robot.2021.103983
18 H. Amase, Y. Nishioka, and T. Yasuda: Proc. Int. Conf. Machine Automation (2015) 2559. https://doi.org/10.1109/ICMA.2015.7237890
19 M. Arfaee, J. Kluin, and J. T. B. Overvelde: Proc. IEEE Int. Conf. Soft Robot. (2023) 1. https://doi.org/10.1109/RoboSoft55895.2023.10122046
20 V. Sanchez, C. J. Payne, D. J. Preston, J. T. Alvarez, J. C. Weaver, A. T. Atalay, M. Boyvat, D. M. Vogt, R. J. Wood, G. M. Whitesides, and C. J. Walsh: Adv. Mater. Technol. **5** (2020) 2000383. https://doi.org/10.1002/admt.202000383
21 R. Uramune, H. Ishizuka, T. Hiraki, Y. Kawahara, S. Ikeda, and O. Oshiro: IEEE Access **10** (2022) 16830. https://doi.org/10.1109/ACCESS.2022.3141385
22 M. R. Mitchell, C. McFarland, and M. M. Coad: Proc. IEEE Int. Conf. Soft Robot. (2023) 1. https://doi.org/10.1109/RoboSoft55895.2023.10122112
23 W. Kim, H. Park and J. Kim: IEEE Robot. Autom. Lett. **6** (2021) 2603. https://doi.org/10.1109/LRA.2021.3062012
24 J. C. Yeo, H. K. Yap, W. Xi, Z. Wang, C. H. Yeow, and C. T. Lim: Adv. Mater. Technol. **1** (2016) 1600018. https://doi.org/10.1002/admt.201600018
25 C.-Y. Wu, W. H. Liao and Y.-C. Tung: Lab Chip **11** (2011) 1740. https://doi.org/10.1039/c0lc00620c
26 U. Cluha, S. G. Nurzaman, F. Clemens, and F. Iida: Sensors **14** (2014) 12748. https://doi.org/10.3390/s140712748
27 A. Koivikko, E. Sadeghian Raei, M. Mosallaei, M. Mäntysalo and V. Sariola: IEEE Sens. J. **18** (2018) 223. https://doi.org/10.1109/JSEN.2017.2765745
28 Y. L. Park, B. R. Chen, and R. J. Wood: IEEE Sens. J. **12** (2012) 2711. https://doi.org/10.1109/JSEN.2012.2200790
29 B. Li, Y. Gao, A. Fontecchio, and Y. Visell: Smart Mater. Struct. **25** (2016) 1. https://doi.org/10.1088/0964-1726/25/7/075009
30 M. K. S. Verma, A. Majumder, and A. Ghatak: Langmuir **22** (2006) 10291. https://doi.org/10.1021/la062516n
31 Y. Hashimoto, T. Usui, H. Ishizuka, S. Ikeda, and O. Oshiro: Jpn. J. Appl. Phys. **60** (2021) SCCL12. https://doi.org/10.35848/1347-4065/abec60

32 T. Usui, H. Ishizuka, T. Hiraki, Y. Kawahara, S. Ikeda, and O. Oshiro: Jpn. J. Appl. Phys. **60** (2021) SCCL11. https://doi.org/10.35848/1347-4065/abec8d
33 1-Axis Soft Flexible Sensor: https://www.nitto.com/us/en/nbt/products/1-axis-soft-flex-sensor/ (accessed April 2024).
34 L. Johnston, J. Yang, J. Han, K. Kalantar-Zadeh, and J. Tang: J. Mater. Chem. C **10** (2022) 921. https://doi.org/10.1039/d1tc04877e
35 M. D. Dickey, R. C. Chiechi, R. J. Larsen, E. A. Weiss, D. A. Weitz, and G. M. Whitesides: Adv. Funct. Mater. **18** (2008) 1097. https://doi.org/10.1002/adfm.200701216
36 J. Li, L. Wang, X. Wang, Y. Yang, Z. Hu, L. Liu, and Y. Huang: ACS Appl. Mater. Interfaces. **12** (2020) 1427. https://doi.org/10.1021/acsami.9b15546
37 J. Chen, J. Zhang, Z. Luo, J. Zhang, L. Li, Y. Su, X. Gao, Y. Li, W. Tang, C. Cao, Q. Liu, L. Wang, and H. Li: ACS Appl. Mater. Interfaces **12** (2020) 22200. https://doi.org/10.1021/acsami.0c04709
38 H. Godaba, A. Sajad, N. Patel, K. Althoefer, and K. Zhang: Proc. IEEE/RSJ Int. Conf. Intell. Robots Syst. (2020) 8716. https://doi.org/10.1109/IROS45743.2020.9341554
39 J. C. Yeo, H. K. Yap, W. Xi, Z. Wang, C.-H. Yeow, C. T. Lim: Adv. Mater. Technol. **1** (2016) 1600018. https://doi.org/10.1002/admt.201600018
40 J. Chen, J. Zheng, Q. Gao, J. Zhang, J. Zhang, O. M. Omisore, L. Wang, and H. Li.: Appl. Sci. **8** (2018) 345. https://doi.org/10.3390/app8030345
41 Z. Sun, S. Wang, Y. Zhao, Z. Zhong, and L. Zuo: Adv. Intell. Syst. **4** (2022) 2200089. https://doi.org/10.1002/aisy.202200089
42 G. Li, F. Sun, H. Chen, Y. Jin, A. Zhang, and J. Du: ACS Appl. Mater. Interfaces **13** (2021) 56961. https://doi.org/10.1021/acsami.1c17514